Results in Physics 9 (2018) 1578–1584

Contents lists available at ScienceDirect

Results in Physics

journal homepage: www.elsevier.com/locate/rinp

High sensitive temperature sensor silicon-based microring resonator using the broadband input spectrum

Iraj S. Amiri[a,b,*], M.M. Ariannejad[c], S. Daud[d,e], P. Yupapin[a]

[a] Computational Optics Research Group, Advanced Institute of Materials Science, Ton Duc Thang University, Ho Chi Minh City, Viet Nam
[b] Faculty of Applied Sciences, Ton Duc Thang University, Ho Chi Minh City, Viet Nam
[c] Photonics Research Centre, University of Malaya, 50603 Kuala Lumpur, Malaysia
[d] Laser Center, Ibnu Sina Institute for Scientific & Industrial Research, Universiti Teknologi Malaysia, 81310 Johor Bahru, Johor, Malaysia
[e] Department of Physics, Faculty of Science, Universiti Teknologi Malaysia, 81310 Johor Bahru, Johor, Malaysia

ARTICLE INFO

Keywords:
Temperature sensor
Silicon oxynitride (SiON)
Microring resonator (MRR)

ABSTRACT

A sensitivity enhanced optical temperature sensor has been investigated and developed based on a silicon oxynitride (SiON) waveguide microring resonator (MRR). The broadband supercontinuum (SC) output from a fiber laser cavity is injected into the input port of the MRR, where the output was detected at the drop port of MRR. The results can be useful for the sensor-based waveguide devices, where the applications such as the temperature sensors can be realized. The temperature sensor has been fabricated in an MRR-silicon base structure. Experimental characterization of inserting the SC as input source into the MRR as the temperature sensors were carried out. The advantage of using the SC as input source is that the sensor covers a wide range of wavelengths, thus sensing the temperature changes in the wide wavelength ranges which can extend the sensing device applications. This study opens a way to apply optical sensors by using broadband SC as a source for manufacturing temperature environments sensors within the MRR waveguide structures. This will enhance the ability of the current temperature sensors to function at different and long wavelength band.

Introduction

Various applications in material and laser processing, range finding, fiber sensor, medicine, and long-range optical communications can be realized by the usage of large energy pulsed lasers. Q-switching is a kind of optical modulation in the laser cavity. An effective way to deliver large energy pulses can be indicated by the quality factor (Q_{factor}), where it is a result of releasing of the energy stored in an active medium within a very short time [1]. Q-switched lasers can be generated and presented in both passive and active systems, where there are advantages of using active Q-switching than passive cases such as controllable repetition rate and long-term stability [2]. For the device applications such as modulators and acoustic sensors, the active Q-switching has drawbacks of low damage threshold, expensive and low peak power than the active cases [3,4]. The advantages of, low cost, flexibility, simple design and compactness can be achieved by passive Q-switching [5]. Yu Chen et al., investigated Q-switched erbium-doped fiber laser for the applications of broadband and tunable lasers [6] (see Fig. 1).

In order to generate the femtosecond pulses, the technique as nonlinear polarization rotation (NPR) can be utilized [7]. This technique is applicable in mode-locked fiber lasers. Other applications of the technique can be as amplitude-equalization and suppression of super-mode noise in the mode-locked laser systems [8]. The suppress super-mode noise in a multiwavelength mode-locked laser system has been reported by Ran et al. using the NPR technique [9]. Current investigation focusses on solitary wave applications in fiber lasers [10]. The soliton formation occurs due to the mechanism governed between the nonlinear optical Kerr effect and the anomalous system dispersion [11–14]. In a system with normal dispersion, soliton can be generated due to the mutual interaction, where the laser gain effective bandwidth filtering is of importance [15].

There are different soliton shaping mechanism which can differentiate between different solitons which different properties and features, where the kind of solitons achieved in an anomalous dispersion show optical spectrum with clear sidebands. The other solitons generated in normal dispersion experience a steep spectral edge. Several investigations have carried on multiwavelength cavity lasing in the room temperature medium using mode-locked erbium-doped fiber ring laser (ML-EDFRL). In these investigations, the gain filtering mechanism

* Corresponding author at: Ton Duc Thang University, Ho Chi Minh City, Viet Nam.
E-mail address: irajsadeghamiri@tdt.edu.vn (I.S. Amiri).
URL: https://scholar.google.com/citations?hl=en&user=rM8jFG4AAAAJ&view_op=list_works&sortby=pubdate (I.S. Amiri).

https://doi.org/10.1016/j.rinp.2018.05.004
Received 27 March 2018; Received in revised form 1 May 2018; Accepted 2 May 2018
Available online 05 May 2018

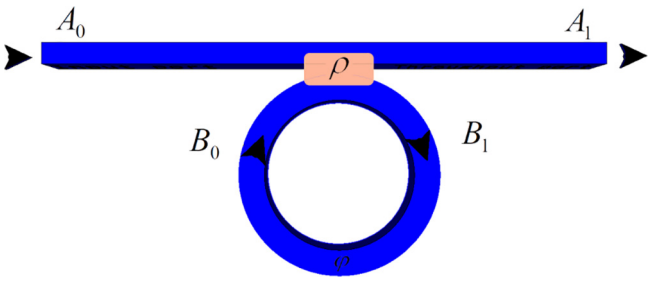

Fig. 1. Single coupler MRR.

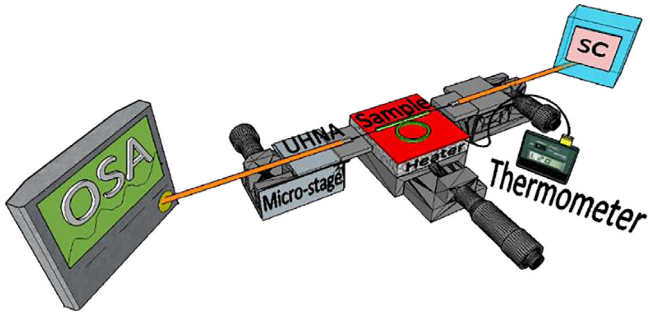

Fig. 3. The micro-stage experiment set up with waveguide loaded on the middle stage so that it is coupled to fibers as input (SC) and output (OSA).

[16,17], multiple gain media [18,19], temporal-spectral multiplexing [20] and interchannel multiple four-wave mixing [16] have been utilized to perform the experiments. The main challenges of the mentioned laser systems were the poor tunability and complicity of the designs. S.L. Shapiro and R.R. Alfano have demonstrated the use of Supercontinuum (SC) in the 1970 s, where the broadening of laser spectrum has attracted many researchers [21,22]. The SC has found many applications in telecommunications [23], optical coherence tomography [24], spectroscopy [25], frequency metrology [24], and device characterization [26]. The SC generation undergoes complicated classical nonlinear optical and physical phenomenon which involves cross-phase modulation (CPM), self-phase modulation (SPM), stimulated Raman scattering (SRS) and four-wave mixing (FWM) [27].

The optical sensors have been investigated in many years due to several interests such as immunity to electromagnetic interference, and compact size compared with the traditional electric types [28]. Most of the used optical sensors are based on optical fibers such as Bragg gratings. These have many advantages such as high sensitivity and low cost, where there are limitations for the sensors in integrated devices [29]. To overcome the problem, new sensing devices have been built up and developed such as the polymer bending waveguides [30], microring resonator (MRR) [13,31–34] and multimode interferometer [35]. The MRR is desired due to their compact size, and also great wavelength-selective capacities. These are highly sensitive to the environment refractive index changes in the vicinity of the structure and are very practical use in integrated photonics circuits for the applications such as temperature sensors [36,37].

Compared to the traditional sensors, MRRs have a faster response due to owing smaller size and compact designs. MRRs can be either attached or embedded in different mediums enable to improve the real-time monitoring and control. These are resonance structures for the input power provided the circumference of the MRR is equal to an integer number of the center wavelength. The steady state relation of the input and output powers of the MRRs can be found in references [38].

The SC generation requires a mode-locked pulse laser as the seeding source [39–41]. It is interesting to investigate the potential of a single pulse seed laser to produce multiple SCs. Multiple SCs generation based on single pulse seed laser offers a further reduction in the implementation cost, thus introduces substantial simplification in size compared to the standard SC setup. The broadband spectra as SC can be generated by applying the mode-locked laser pulse and input into the waveguide structures [42,43]. Wide bandwidth SC generation has been demonstrated in microstructured fibers [44], highly nonlinear chalcogenide planar waveguide [45], periodically poled lithium niobate [46], and Si [47]. MRRs are a key component in modern optical networks [48–50]. Their size allows high-density integration in optical photonic circuits due to the use of high index contrast. MRR based filters in wavelength division multiplexing are considered as effective devices in this technology [51–53]. Many types of selective filters have been investigated and utilized such as those with very small channel spacing suitable for the integration systems [54]. These filters can be fabricated using different materials such as glass [54], glass–polymer [55], Si-SiO2 [56], SiON [57], and GaInAsP/InP [58–61].

The MRRs exabit high contrast waveguides, where a higher refractive index contrast causes lower bending losses and higher free spectral range of the filtered input spectrum. The scattering losses and the tolerance sensitivity are the major drawbacks of the MRR waveguides. These can be managed and reduced by using the plasma-enhanced chemical vapor deposition technique which can be used to fabricate waveguides such as SiON. This technique can fabricate waveguides with lower losses, therefore it is desired for design and fabrication of compact devices in an integrated circuit system for the application of wavelength-division multiplexing [62]. MRRs which are made based on silicon wafers have been used in several applications such as bandpass filters, wavelength-division multiplexing systems, and add/drop filters [63]. In reference [64], the authors have investigated

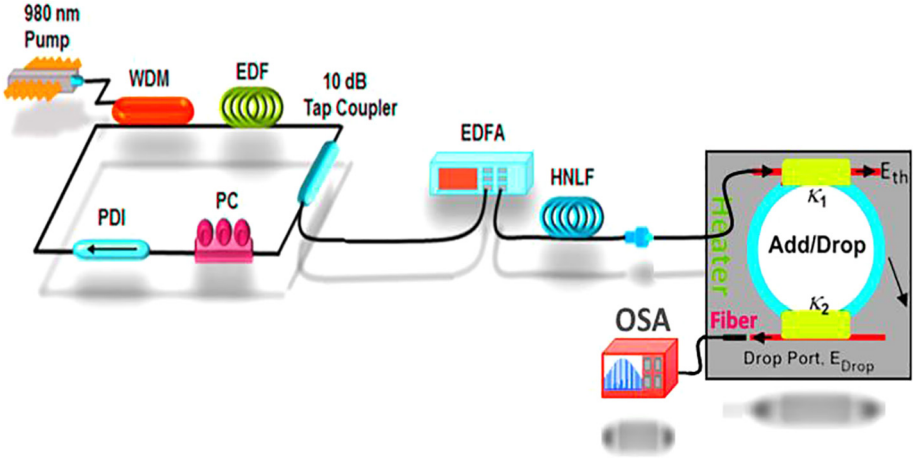

Fig. 2. Experimental set-up of the temperature sensor with MRR.

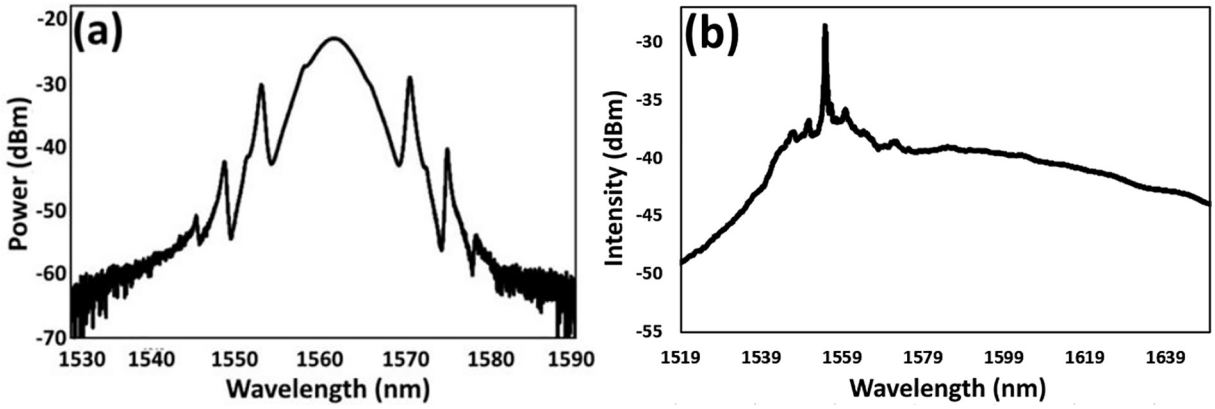

Fig. 4. (a) Mode-locked spectrum generated by the laser cavity, (b) the supercontinuum generated at the output of the HNLF.

the generation of signals with 0.4 nm bandwidth. The MRRs can be utilized as an integrated device in a fiber laser setup or they can be outside of the setup. To generate polarization independent multi-wavelength or dual wavelength the use of the MRRs outside of the laser cavity is recommended. This configuration has other advantages such as the tunability and stability of the generated output wavelengths, where it makes the MRRs most ideal choices for the wavelength selective filter devices. In reference [65], Amiri et al. has presented a similar experiment setup to filter out the input supercontinuum pulse generated from the fiber laser setup for the tunable dual-wavelength applications within the ranges 1520 and 1640 nm, while in the presented work, the fabricated SiON-MRR with 1.27 mm diameter is utilized as a temperature sensor.

Generation of mode-locked laser and supercontinuum

The experiment setup of the temperature sensor has been shown in Fig. 2. The fiber laser system is divided into two main stages. The first stage consists of a ring cavity to induce mode-locking operation. A 50 cm length of Erbium-doped fiber (EDF) is performed as the gain medium in the cavity. The EDF is pumped by a 980 nm laser diode through a 980/1550 nm wavelength division multiplexer (WDM). The EDF is then connected to polarization dependent isolator (PDI) and followed by a polarization controller (PC). The function of the PDI is to ensure unidirectional propagation in the cavity and act as a polarizer, while the function of the PC is to control the polarization state in the ring cavity. The incorporation of the PDI-PC induces the NPR effect in the cavity. The ring cavity is completed by using a 90/10 tap coupler in which 90% of the generated laser power oscillates in the cavity whilst the remaining 10% is extracted as an input to the Erbium-doped fiber amplifier (EDFA). The amplified laser emission then propagates through a 100 m long HNLF to induce the SC effect. The results have been analyzed by using an optical spectrum analyzer with 0.02 nm resolution, a 12.5 GHz wideband photodetector (covering the operating wavelength range from 1.5 μm to 2.1 μm), a 500 MHz oscilloscope, an autocorrelator resolution, and a radio-frequency (RF) analyzer. An MRR is then connected to the output port of the HNLF to slice the SC spectrum. Compared to the superluminescent diodes, the SC owning a broader spectrum and shorter coherent length. The coherent length of SC is 3–7 μm, while it is 20 μm for the superluminescent diodes, thus improvement of temperature measurement accuracy is expected for SC applications. The micro-stage that has been used for waveguide alignment was precise so that it could make sure the coupling of light could be more efficient. The middle stage has the feature that can put the ceramic positive temperature coefficient (PTC) heater and thermometer for verification of the exact changes of temperature so that the desired temperature was measured by thermometer to be sure the thermometer sensor was touching the waveguide to measure the correct temperature.

A strong peak due to the pump frequency can be observed at the through port of the microring resonator. The peak is often 20 dB above the adjacent comb lines, therefore the power transfer to the comb is poor [66,67]. To avoid this issue, the silicon nitride microring resonator could be fabricated with a drop port, thought a drop port geometry has been widely used in optical add/drop filters [68].

Fig. 3 illustrates the whole setup from the stage side and by referring the source (SC) that could produce the wide wavelength spectrum so that the study of temperature on changing the MRR resonance could be possible by this technique.

The PTC heater can be used in this experiment by controlling the voltage so that the desired temperature would be issued. The thermometer was the great help to check and register all the changes base on the live data. The source (SC) was producing a wide range spectrum so that the changes in resonance would be novel and more effective in this case. This application of MRR is very interesting in case of industrial and in communication methods. The sensitivity of the waveguides (MRR) went under the evaluation where the source of the heat never engages with waveguide directly (for example heating source doesn't place above the waveguide holder).

Results and discussion

A stable passively mode-locked seed spectrum is attained at a threshold pump power level of 65 mW, based on the NPR effect from the ring cavity. Fig. 4(a) shows the mode-locked fiber laser spectrum at the 10% port of the optical tap-coupler at a pump power level of 130 mW, where the Fig. 4(b) shows the generated supercontinuum output from the HNLF after the mode-locked pulse input into the HNLF.

The OSA1/YOKOGAWA AQ6370B is utilized for the spectrum analysis. A 3 dB coupler is used to couple the output from the MRR to the OSA. It has a 10 cm length single mode fiber (SMF). The OSA is used to show and monitor the generated frequency comb from the MRR which has a refractive index of 1.513 and footprint of $3 \times 5\ mm^2$. As can be seen from the Fig. 5, the SC is filtered by the MRR through the wavelength range 1519 to 1650 nm. The FSR shows a wavelength range of 0.39 (48.7 GHz) to 0.45 nm (56 GHz).

Free spectral range (FSR)

An important parameter that characterizes the MRR structure for sensing applications is the free spectral range (*FSR*). The *FSR* parameter determines the spacing distance between two resonance peaks of the micro-resonator structure, and it is defined as below (Eq. (1)):

$$FSR = \frac{\lambda_{res}^2}{n_{eff}(2\pi R)} \tag{1}$$

where λ_{res} represents the resonance wavelength, n_{eff} is the effective

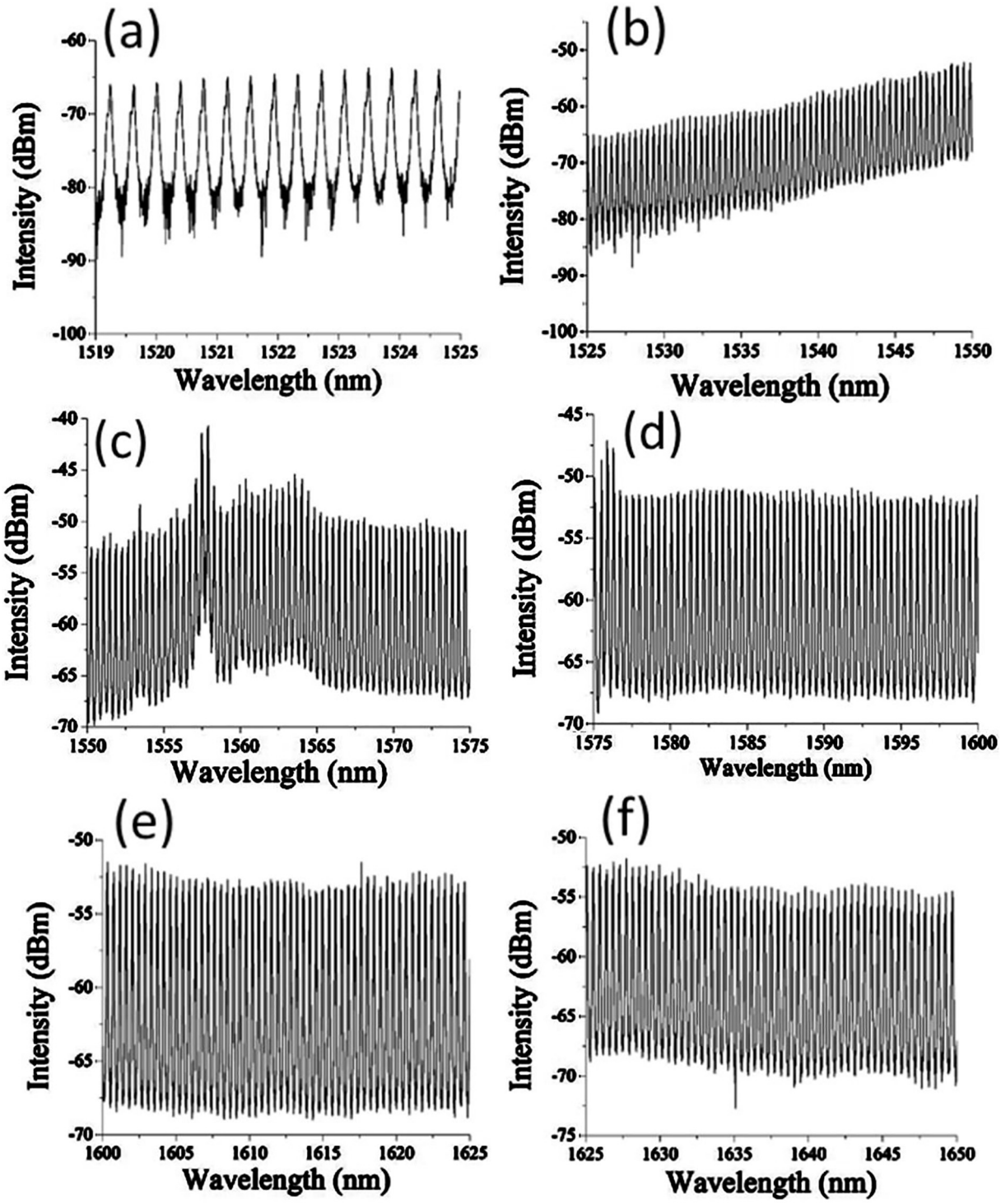

Fig. 5. Advanced frequency combs in SiON-MRR. Sub-100 GHz spacing SiON-MRR. Micrographs of the (a) 48.7 (b) 50, (c) 51.2, (d) 52.4, (e) 53.7 and (f) 56.2 GHz FSR.

refractive index of the MRR and R is the radius dimension of the MRR. The $2\pi R$ term is the circumference of the MRR structure. Clearly, the FSR value will vary as different regions of the spectrum. A narrow FSR distance will exist at shorter wavelengths, such as in the visible spectrum (at 700–800 nm) compared to the wider FSR values found at a longer wavelength region (e.g. In the Near Infrared (NIR) region between A = 800–2500 nm).

Effective refractive index (n_{eff})

The effective refractive index plays a major role in the MRR optical sensing. There are several software packages that are commercially available to calculate the effective refractive index of a system. The effective refractive index is defined as:

$$n_{eff} = \frac{\beta\lambda}{2\pi} \quad \text{or} \quad n_{eff} = \frac{\beta}{k} \tag{2}$$

In Eq. (2), β represents the propagation constant, λ is the

Table 1
Important parameters calculated in the SiON-MRR within injecting supercontinuum as a source within the 23.4°c temperature.

Temp 23.4°c	Wavelength					
	1520 nm	1540 nm	1570 nm	1590 nm	1615 nm	1630 nm
FSR(nm)	0.39	0.39	0.41	0.42	0.43	0.45
FWHM	0.07	0.085	0.095	0.1	0.105	0.105
Q_{factor}	2.2×10^4	1.8×10^4	1.6×10^4	1.5×10^4	1.5×10^4	1.5×10^4
Finesse	5.57	4.6	4.31	4.2	4.09	4.2
Δf(GHz)	48.7	48.7	51.2	52.4	53.7	56.2

Table 2
Important parameters calculated in the SiON-MRR within injecting supercontinuum as a source within different temperature.

Wavelength	Temperature			
	25 °c	26 °c	27 °c	28 °c
FSR(nm)	0.42	0.4	0.42	0.4
FWHM	0.1	0.1	0.15	0.075
Q_{factor}	1.5×10^4	1.5×10^4	1.03×10^4	2.06×10^4
Finesse	4.2	4	2.8	5.3
Δf(GHz)	52.4	49.95	52.44	49.94

wavelength (nm), k is the reciprocal of wavenumber. In this work, finite-difference-time-domain (FDTD) technique simulation Lumerical was utilized as a tool to determine the effective refractive index of waveguide structures. This fundamental can be used in case of sensing within optical MRR. The interaction between the surface of the MRR can make the change in the effective index of the material. This change influences the resonance wavelength peak place. The sensing equation can be defined as below:

$$\frac{\Delta\lambda}{\lambda} = \frac{\Delta n_{eff}}{n_{eff}} \tag{3}$$

where $\Delta\lambda$is the resonance wavelength shift or displacement; $\lambda$is the resonance wavelength for a particular mode; $\Delta n_{eff}$is the effective refractive index changes, and $n_{eff}$is the effective refractive index of the MRR [69–71]. According to the Eq. (3), the resonance wavelength shifts linearly, dependent on changes in the effective index of the MRR. Losses and coupling coefficients are relevant to the width at half maximum (FWHM) in the spectrum of resonance in the all-pass MRRs. The FSR can be expressed by:

$$FSR = \frac{\lambda^2}{n_g L} \tag{4}$$

where the round-trip length is defined by L and n_g is the group index. The dispersion of the waveguide can be considered by the group index and is defined by

$$n_g = n_{eff} - \lambda_0 \frac{dn_{eff}}{d\lambda} \tag{5}$$

The ratio of FSR and resonance width is defined as finesse whereas,

$$Finesse = \frac{FSR}{FWHM} \tag{6}$$

Spacing is a key factor to describe the sharpness of resonances. The sharpness of the resonance within the relative to the central frequency can define the Q_{factor} which is described by:

$$Q_{factor} = \frac{\lambda_{res}}{FWHM} \tag{7}$$

The number of round-trips made by the energy in the resonator can define the finesse and Q_{factor} before being lost due to the bus waveguides and internal loss. Table 1 is illustrating the important parameters in 23.4°c such as FSR, FWHM, Q_{factor}, finesse, and Δf. The FSR and Δf trend is increasing by the increase of wavelength also the FWHM following this trend. Q_{factor} would decrease by the increasing the wavelength. In Table 2 it has been shown the effect of the changes in temperature, the Q_{factor} increase by the increase of the temperature through the FSR is almost same and finesse has decrees till 27 °c then in 28 °c it increased.

The variation of temperature due to the variation of heat produced by the PTC ceramic heater has been measured by a thermometer. This measurement indicates a linear change of the temperature from a starting point of 24 °C with the step of 1°Celcius per 30 s invervals. The spectrum after the MRR and splicing showing an insensitive wavelength shifting within the increase of temperature, where the ampliture changes dramatically. The wavelength shifting occurs if the high temperature variation applied. It is considerable as a sensitive temprature sensor in case of using the SC as the source and splicing by MRR in SiON material. By increasing the temprature the power decreases as almost 10 dBm. In Fig. 6 the power fluctuation has been illustrated.

The power coupling coefficient between the waveguide and the ring can be estimated from the bandwidth double-notch feature of the resonant spectrum cause by the weak split of resonances and it is a weak reflection inside the MRR so that the surface roughness also can be affected by the back reflections [72].

Conclusion

A temperature sensor base on SiON-MRR presented by launching SC laser pulses as the input source. Moreover, the MRR has a small footprint of $3 \times 5\,mm^2$. The FSR achieved was between 0.39 till 0.45,

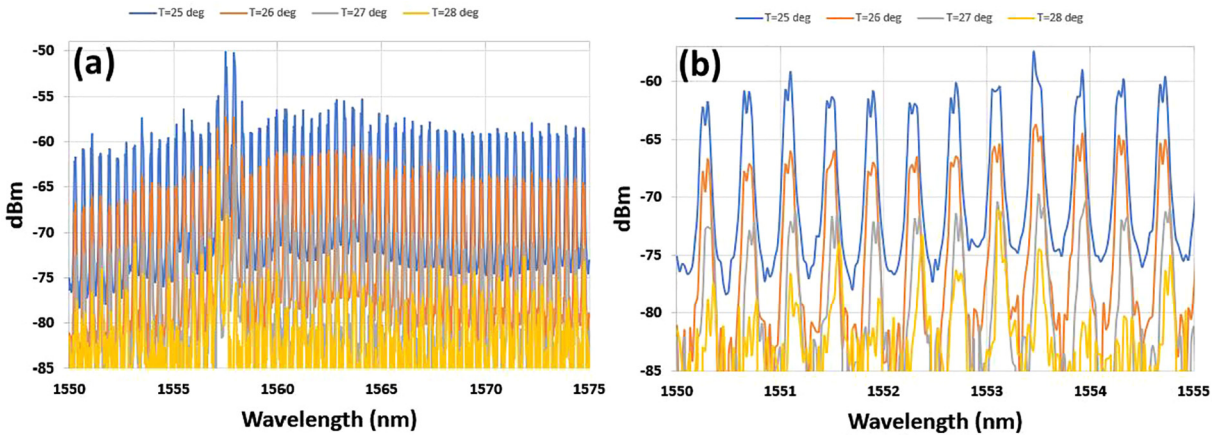

Fig. 6. The amplitude variation between (a) 1550–1575 nm (b) 1550–1555 nm due to the temperature variations.

where the Q_{factor} of the MRR with diameters of 1.27 mm ranges from 1.5×10^4 to 2.2×10^4. The Q_{factor} increase by the increase of the temperature, though the FSR is almost same and finesse has decrees till 27 °c then in 28 °c it increased. The temperature sensor shows insensitive wavelength shifting as the temperature increases but it shows a significant change in the output power even if the temperature changes are very small. The sensor shows a high sensitivity to the temperature variation by the output power changes which means it can detect a very small change in the output power due to the small changes in the temperature.

Appendix A. Supplementary data

Supplementary data associated with this article can be found, in the online version, at http://dx.doi.org/10.1016/j.rinp.2018.05.004.

References

[1] Ryvkin B, Avrutin E, Kostamovaara J, Kostamovaara J. Laser diode structures with a saturable absorber for high-energy picosecond optical pulse generation by combined gain-and Q-switching. Semicond Sci Technol 2017;32:025015.
[2] Scott AM. Construction and passive Q-switching of a ring-cavity erbium-doped fiber laser using carbon nanotubes as a saturable absorber. Rose Hulman Inst Technol 2017.
[3] Li H, Xia H, Lan C, Li C, Zhang X, Li J, et al. Passively $ Q $-switched erbium-doped fiber laser based on few-layer MoS 2 saturable absorber. IEEE Photonics Technol Lett 2015;27:69–72.
[4] Hassan H, Ariannejad M, Safaei R, Amiri I, Ahmad H. Mode-locked Erbium-doped fiber laser generation using hybrid ZnO/GO saturable absorber. IOP Conference Series: Materials Science and Engineering. 2017. p. 012046.
[5] Luan C, Yang K, Zhao J, Zhao S, Li G, Li D, et al. Highly efficient passively Q-switched solid-state 2 μm laser with monolayer graphene. Opt Quant Electron 2015;47:3525–31.
[6] Chen Y, Zhao C, Chen S, Du J, Tang P, Jiang G, et al. Large energy, wavelength widely tunable, topological insulator Q-switched erbium-doped fiber laser. IEEE J Sel Top Quantum Electron 2014;20:315–22.
[7] Cao Y, Jia D, Liu T, Wang Z, Yang T. Ultra-wide square pulses generation in a Yb-doped fiber laser based on nonlinear polarization rotation effect. Conference on Lasers and Electro-Optics Pacific Rim (CLEO-PR). 2017. p. 1–3.
[8] Li Z, Lou C, Chan KT, Li Y, Gao Y. Theoretical and experimental study of pulse-amplitude-equalization in a rational harmonic mode-locked fiber ring laser. IEEE J Quantum Electron 2001;37:33–7.
[9] Pan S, Lou C. Stable multiwavelength dispersion-tuned actively mode-locked erbium-doped fiber ring laser using nonlinear polarization rotation. IEEE Photonics Technol Lett 2006;18:1451–3.
[10] Zhao L, Tang D, Wu J. Gain-guided soliton in a positive group-dispersion fiber laser. Opt Lett 2006;31:1788–90.
[11] Alizadeh F, Hashim M, Ahmad H, Amiri I. InGaAsP/InP microring resonator (MRR) waveguide used to generate soliton comb with tunable channel spacing. J Comput Theor Nanosci 2016;13:4829–34.
[12] Amiri I, Ahmad H, Ghasemi M, Ismail M, Aidit S, Soltanian M, et al. Silicon-based microring resonators for multi-solitons generation for THz communication. Opt Quant Electron 2016;48:415.
[13] Amiri I, Ariannejad M, Ghasemi M, Ismail M, Azzuhri S, Nafarizal N, et al. Visible wireless communications using solitonic carriers generated by microring resonators (MRRs). Iranian J Sci Technol, Trans A: Sci 2016:1–7.
[14] Amiri I, Al-Khafaji HM. Widely wavelength-tunable solitonic pulse generation using InGaAsP/InP microring resonators. Communications 2016;1:9–15.
[15] Chong A, Renninger WH, Wise FW. All-normal-dispersion femtosecond fiber laser with pulse energy above 20nJ. Opt Lett 2007;32:2408–10.
[16] Chen L, Town G, Cortes P, LaRochelle S, Smith P. Dual-wavelength, actively mode-locked fibre laser with 0.7 nm wavelength spacing. Electron Lett 2000;36:1.
[17] Amiri I, Ariannejad M, Ghasemi M, Ahmad H. Transmission performances of solitons in optical wired link. Appl Comput Inform 2017;13:92–9.
[18] Pudo D, Chen LR. Actively modelocked, quadruple-wavelength fibre laser with pump-controlled wavelength switching. Electron Lett 2003;39:272–4.
[19] Amiri I, Ariannejad M, Ahmad H, Yupapin P. Simulation of mode lock lasers using microring resonators integrated with InGaAsP saturable absorbers. Indian J Phys 2017:1–5.
[20] Lou J, Carruthers T, Currie M. 4× 10 GHz mode-locked multiple-wavelength fiber laser. IEEE Photonics Technol Lett 2004;16:51–3.
[21] Alfano R, Shapiro S. Observation of self-phase modulation and small-scale filaments in crystals and glasses. Phys Rev Lett 1970;24:592.
[22] Alfano R, Shapiro S. Emission in the region 4000 to 7000 Å via four-photon coupling in glass. Phys Rev Lett 1970;24:584.
[23] Dudley JM, Genty G, Coen S. Supercontinuum generation in photonic crystal fiber. Rev Modern Phys 2006;78:1135.
[24] Washburn BR, Diddams SA, Newbury NR, Nicholson JW, Yan MF, Jørgensen CG. Phase-locked, erbium-fiber-laser-based frequency comb in the near infrared. Opt Lett 2004;29:250–2.
[25] Shah J. Ultrafast spectroscopy of semiconductors and semiconductor nanostructures. Springer Science & Business Media; 2013.
[26] Neal R, Charlton M, Parker G, Finlayson C, Netti M, Baumberg J. Ultrabroadband transmission measurements on waveguides of silicon-rich silicon dioxide. Appl Phys Lett 2003;83:4598–600.
[27] Brambilla G, Koizumi F, Finazzi V, Richardson D. Supercontinuum generation in tapered bismuth silicate fibres. Electron Lett 2005;41:795–7.
[28] Kim H, Jang E, Lee S. Electrooptic temperature sensor based on a Fabry-Perot resonator with a liquid crystal film. IEEE Photon Technol Lett 2006;18:905.
[29] Rao Y-J, Ran Z-L, Liao X, Deng H-Y. Hybrid LPFG/MEFPI sensor for simultaneous measurement of high-temperature and strain. Opt Express 2007;15:14936–41.
[30] Remouche M, Mokdad R, Chakari A, Meyrueis P. Intrinsic integrated optical temperature sensor based on waveguide bend loss. Opt Laser Technol 2007;39:1454–60.
[31] Goykhman I, Desiatov B, Levy U. Ultrathin silicon nitride microring resonator for biophotonic applications at 970 nm wavelength. Appl Phys Lett 2010;97:081108.
[32] Amiri I, Ariannejad M, Ahmad H. Tunable multi-wavelength generation using InGaAsP/InP microring resonator with detectable resonance wavelength shift due to a sensing cladding section. Chin J Phys 2016;54:780–7.
[33] Amiri IS, Ariannejad M, Kouhdaragh V, Seyedi S, Yupapin P. Microring resonator made by ion-exchange technique for detecting the CO2, H2O, and NaCl as cladding layer. J King Saud Univ Sci 2017.
[34] Amiri IS, Ariannejad M, Tajdidzadeh M, Sorger VJ, Ling X, Yupapin P. Fast and slow light generated by surface plasmon wave and gold grating coupling effects. Indian J Phys 2018:1–10.
[35] Irace A, Breglio G. All-silicon optical temperature sensor based on multi-mode interference. Opt Express 2003;11:2807–12.
[36] Kwon M-S, Steier WH. Microring-resonator-based sensor measuring both the concentration and temperature of a solution. Opt Express 2008;16:9372–7.
[37] Orghici R, Lützow P, Burgmeier J, Koch J, Heidrich H, Schade W, et al. A microring resonator sensor for sensitive detection of 1, 3, 5-trinitrotoluene (TNT). Sensors 2010;10:6788–95.
[38] Okamoto K. Fundamentals of optical waveguides. Academic press; 2010.
[39] Kubat I, Bang O. Multimode supercontinuum generation in chalcogenide glass fibres. Opt Express 2016;24:2513–26.
[40] Kurkov A, Sholokhov E, Sadovnikova YE. All-fiber supercontinuum source in the range of 1550–2400 nm based on telecommunication multimode fiber. Laser Phys Lett 2011;8:598–600.
[41] Kulkarni OP, Alexander VV, Kumar M, Freeman MJ, Islam MN, Terry Jr FL, et al. Supercontinuum generation from ~ 1.9 to 4.5 μmin ZBLAN fiber with high average power generation beyond 3.8 μm using a thulium-doped fiber amplifier. JOSA B 2011;28:2486–98.
[42] Cundiff ST, Weiner AM. Optical arbitrary waveform generation. Nat Photonics 2010;4:760–6.
[43] Takesue H, Inoue K. 1.5-μm band quantum-correlated photon pair generation in dispersion-shifted fiber: suppression of noise photons by cooling fiber. Opt Express 2005;13:7832–9.
[44] Dyer SD, Stevens MJ, Baek B, Nam SW. High-efficiency, ultra low-noise all-fiber photon-pair source. Opt Express 2008;16:9966–77.
[45] Halder M, Fulconis J, Cemlyn B, Clark A, Xiong C, Wadsworth WJ, et al. Nonclassical 2-photon interference with separate intrinsically narrowband fibre sources. Opt Express 2009;17:4670–6.
[46] Clark A, Bell B, Fulconis J, Halder MM, Cemlyn B, Alibart O, et al. Intrinsically narrowband pair photon generation in microstructured fibres. New J Phys 2011;13:065009.
[47] Xiong C, Marshall GD, Peruzzo A, Lobino M, Clark AS, Choi D-Y, et al. Generation of correlated photon pairs in a chalcogenide As2S3 waveguide. Appl Phys Lett 2011;98:051101.
[48] Tanaram C, Teeka C, Jomtarak R, Yupapin P, Jalil M, Amiri I, et al. ASK-to-PSK generation based on nonlinear microring resonators coupled to one MZI arm. Procedia Eng 2011;8:432–5.
[49] Soltanian M, Ahmad H, Khodaie A, Amiri I, Ismail M, Harun S. A stable dual-wavelength Thulium-doped fiber laser at 1.9 μm using photonic crystal fiber. Sci Rep 2015;5:14537.
[50] Amiri I, Alavi S, Ali J. High-capacity soliton transmission for indoor and outdoor communications using integrated ring resonators. Int J Commun Syst 2015;28:147–60.
[51] Amiri I, Soltanian M, Alavi S, Ahmad H. Multi wavelength mode-lock soliton generation using fiber laser loop coupled to an add-drop ring resonator. Opt Quant Electron 2015;47:2455–64.
[52] Alavi S, Amiri I, Ahmad H, Supa'at A, Fisal N. Generation and transmission of 3× 3 w-band multi-input multi-output orthogonal frequency division multiplexing-radio-over-fiber signals using micro-ring resonators. Appl Opt 2014;53:8049–54.
[53] Amiri I, Ali J. Optical quantum generation and transmission of 57–61 GHz frequency band using an optical fiber optics. J Comput Theor Nanosci 2014;11:2130–5.
[54] Madsen CK, Zhao JH. Optical filter design and analysis: a signal processing approach. John Wiley & Sons, Inc.; 1999.
[55] Chu ST, Pan W, Suzuki S, Little BE, Sato S, Kokubun Y. Temperature insensitive vertically coupled microring resonator add/drop filters by means of a polymer overlay. IEEE Photonics Technol Lett 1999;11:1138–40.
[56] Little BE, Foresi J, Steinmeyer G, Thoen E, Chu S, Haus H, et al. Ultra-compact Si-SiO 2 microring resonator optical channel dropping filters. IEEE Photonics Technol Lett 1998;10:549–51.
[57] De Brabander GN, Boyd JT, Beheim G. Integrated optical ring resonator with micromechanical diaphragms for pressure sensing. IEEE Photonics Technol Lett

1994;6:671–3.
[58] Rabus D, Hamacher M, Troppenz U, Heidrich H. High-Q channel-dropping filters using ring resonators with integrated SOAs. IEEE Photonics Technol Lett 2002;14:1442–4.
[59] Amiri I, Ali J. Generating highly dark–bright solitons by Gaussian beam propagation in a PANDA ring resonator. J Comput Theor Nanosci 2014;11:1092–9.
[60] Amiri I, Alavi S, Soltanian M, Fisal N, Supa'at A, Ahmad H. Increment of access points in integrated system of wavelength division multiplexed passive optical network radio over fiber. Sci Rep 2015;5:11897.
[61] Soltanian M, Amiri I, Alavi S, Ahmad H. All optical ultra-wideband signal generation and transmission using mode-locked laser incorporated with add-drop microring resonator. Laser Phys Lett 2015;12:065105.
[62] De Ridder RM, Warhoff K, Driessen A, Lambeck PV, Albers H. Silicon oxynitride planar waveguiding structures for application in optical communication. IEEE J Selected Topics Quantum Electron 1998;4:930–7.
[63] Popovíc MA, Barwicz T, Watts MR, Rakich PT, Socci L, Ippen EP, et al. Multistage high-order microring-resonator add-drop filters. Opt Lett 2006;31:2571–3.
[64] Arbabi A, Kang YM, Lu C-Y, Chow E, Goddard LL. Realization of a narrowband single wavelength microring mirror. Appl Phys Lett 2011;99:091105.
[65] Amiri IS, Ariannejad M, Tiu Z, Ooi S, Aidit S, Alizadeh F, et al. A widely tunable dual-wavelength based on a microring resonator filter device. Laser Phys 2018;28:065101.
[66] Engelbrecht R. A compact NIR fiber-optic diode laser spectrometer for CO and CO2: analysis of observed 2f wavelength modulation spectroscopy line shapes. Spectrochim Acta Part A Mol Biomol Spectrosc 2004;60:3291–8.
[67] Mattison D, Jeffries J, Hanson R, Steeper R, De Zilwa S, Dec J, et al. In-cylinder gas temperature and water concentration measurements in HCCI engines using a multiplexed-wavelength diode-laser system: sensor development and initial demonstration. Proc Combust Inst 2007;31:791–8.
[68] Kaminski C, Watt R, Elder A, Frank J, Hult J. Supercontinuum radiation for applications in chemical sensing and microscopy. Appl Phys B 2008;92:367.
[69] Cho S-Y, Jokerst NM. Polymer microrings integrated with thin film ingaas msm photodetectors for sensor-on-a-chip applications. 2006 International Conference on Indium Phosphide and Related Materials Conference Proceedings. 2006.
[70] Amiri I, Naraei P, Ali J. Review and theory of optical soliton generation used to improve the security and high capacity of MRR and NRR passive systems. J Comput Theor Nanosci 2014;11:1875–86.
[71] Amiri I, Alavi S, Fisal N, Supa'at A, Ahmad H. All-Optical Generation of Two IEEE802. 11n Signals for 2$\times $2 MIMO-RoF via MRR System. IEEE Photonics J 2014;6:1–11.
[72] Little BE, Laine J-P, Chu ST. Surface-roughness-induced contradirectional coupling in ring and disk resonators. Opt Lett 1997;22:4–6.